Editors' Suggestion

Membrane-Based Optomechanical Accelerometry

Mitul Dey Chowdhury,[†] Aman R. Agrawal,[†] and Dalziel J. Wilson[*]
Wyant College of Optical Sciences, University of Arizona, Tucson, Arizona 85721, USA

(Received 5 November 2022; revised 21 December 2022; accepted 23 December 2022; published 3 February 2023)

Optomechanical accelerometers promise quantum-limited readout, high detection bandwidth, self-calibration, and radiation-pressure stabilization. We present a simple, scalable platform that enables these benefits with nano-g sensitivity at acoustic frequencies, based on a pair of vertically integrated Si_3N_4 membranes with different stiffnesses, forming an optical cavity. As a demonstration, we integrate an ultrahigh-Q ($> 10^7$), millimeter-scale Si_3N_4 trampoline membrane above an unpatterned membrane on the same Si chip, forming a finesse $\mathcal{F} \approx 2$ cavity. Using direct photodetection in transmission, we resolve the relative displacement of the membranes with a shot-noise-limited imprecision of 7 fm/$\sqrt{\text{Hz}}$, yielding a thermal-noise-limited acceleration sensitivity of 0.6 μg/$\sqrt{\text{Hz}}$ over a 1-kHz bandwidth centered on the fundamental trampoline resonance (40 kHz). To illustrate the advantage of radiation-pressure stabilization, we cold damp the trampoline to an effective temperature of 4 mK and leverage the reduced energy variance to resolve an applied stochastic acceleration of 50 ng/$\sqrt{\text{Hz}}$ in an integration time of minutes. In the future, we envision a small-scale array of these devices operating in a cryostat to search for fundamental weak forces such as dark matter.

DOI: 10.1103/PhysRevApplied.19.024011

I. INTRODUCTION

Cavity optomechanical (COMS) accelerometers employ a micromechanical oscillator as a test mass and an optical microcavity for displacement-based readout. Key advantages over microelectromechanical (MEMS) accelerometers—stemming from the small wavelength of optical fields—include quantum-limited readout, ultrahigh bandwidth; and absolute, traceable calibration [1–4]. An added feature is radiation pressure back-action [5], which in principle can enhance sensor performance by leveraging optical stiffening and damping effects. Both have been studied extensively in the field of cavity optomechanics [6]; however, the predominant use of stiff, radiofrequency nanomechanical resonators in these studies precluded their application to inertial sensing.

First-generation COMS accelerometers used delicate nanofabrication and microassembly techniques to monolithically integrate a relatively large, acoustic frequency test mass with an optical microcavity. Krause *et al.* [1] fabricated a millimeter-scale Si_3N_4 membrane in the near field of a one-dimensional photonic crystal (PtC) cavity, and demonstrated a shot-noise-limited acceleration sensitivity of 10 μg/$\sqrt{\text{Hz}}$ over a bandwidth of 25 kHz. Guzmán *et al.* [2] achieved similar performance by fixing a fiber cavity to a centimeter-scale silica test mass. More recently, Zhou *et al.* [7] formed a flip-chip COMS accelerometer by sandwiching a micromirror against a mass-loaded Si_3N_4 membrane, enabling sub-μg sensitivity over 10 kHz, limited entirely by thermal motion of the test mass.

Here we explore a platform for COMS accelerometery based on a pair of vertically integrated, *unloaded* Si_3N_4 membranes with different stiffnesses, forming an optical cavity. Devices based on this platform are exceptionally easy to fabricate and give access to a panoply of tools developed for Si_3N_4 membranes over the last decade, including frequency tuning [8], PtC patterning (to increase the membrane's reflectivity) [9,10], and access to ultrahigh-Q flexural modes via mode-shape and strain engineering [11,12]. Using a simple trampoline-on-membrane ("TOM") design as an illustration, we demonstrate a $f \sim 10$ kHz, $m \sim 10$ ng test mass with a Q-m product of milligrams. In this unique parameter regime, the test mass exhibits a sub-μg thermal acceleration and at the same time is highly sensitive to radiation pressure. We exploit this feature to cold damp the test mass to several millikelvin, and show how this cooling can be used to detect approximately 10 ng/$\sqrt{\text{Hz}}$ incoherent accelerations.

We note that, besides the study of radiation-pressure-enhanced sensing, development of this platform is motivated by recent proposals to search for weak stochastic accelerations in the acoustic frequency band due to fundamental phenomena, such as spontaneous wave-function collapse and ultralight dark matter [13,14]. These searches can benefit from small-scale arrays of cryogenic optomechanical accelerometers, which call for a simplified approach relative to current technology.

[*]dalziel@arizona.edu
[†]These authors contributed equally to this work.

II. DEVICE CONCEPT

The concept behind our approach is illustrated in Fig. 1. Two dielectric membranes with different stiffnesses are fabricated on opposite sides of the same substrate. (Our membranes are Si_3N_4 and the substrate is Si; however, the concept is agnostic to material.) The substrate represents the inertial reference frame and the membranes represent a pair of spring-mass systems; their displacement $x = x_1 - x_2$ is related to the substrate acceleration a by the difference susceptibility

$$\chi(\omega) = \frac{x(\omega)}{a(\omega)} = \chi_1(\omega) - \chi_2(\omega), \tag{1}$$

where

$$\chi_i(\omega) = \frac{x_i(\omega)}{a(\omega)} \approx \frac{\beta_i}{\omega_i^2 - \omega^2 - i\omega\omega_i/Q_i} \tag{2}$$

is the susceptibility of membrane i, x_i is the displacement of membrane i relative to the substrate, ω_i and Q_i are the resonance frequency and Q factor of membrane i, and $\beta_i \sim 1$ is a unitless factor that depends on the shape of the membrane mode [for a square and a trampoline membrane, $\beta \approx (4/\pi)^2$ and 1, respectively [13,15]].

When the membrane frequencies are different $\omega_1 \neq \omega_2$, it is straightforward to show that $\chi(\omega) \approx \chi_i(\omega)$ for frequencies sufficiently close to resonance $\omega \approx \omega_i$. The dual-membrane system can then be modeled as a canonical spring-mass accelerometer; with the measured displacement yielding an apparent acceleration spectral density

$$S_a(\omega) = |\chi(\omega)|^{-2} S_x^{\text{imp}} + S_a^{\text{th}}, \tag{3}$$

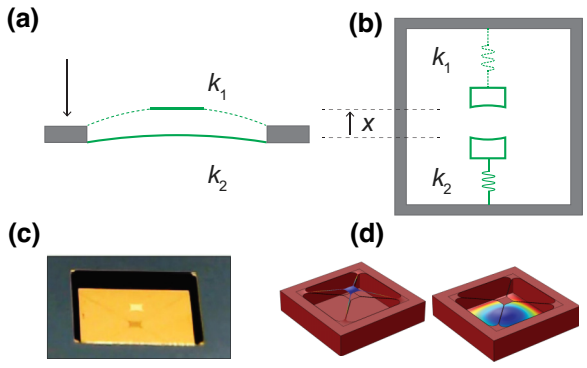

FIG. 1. Concept for dual-membrane accelerometer. (a) A pair of membranes with different stiffnesses attached to a common base respond differently to base acceleration. (b) Each membrane is equivalent to a spring-mass system suspended from a common frame. The membranes also act as Fabry-Pérot end mirrors. (c) Photograph of a TOM accelerometer. (d) Finite-element simulation of the fundamental flexural modes of TOM.

where S_x^{imp} is the displacement readout imprecision and

$$S_a^{\text{th}}(\omega) \approx \frac{4k_B T\omega_i}{\beta_i^2 m_i Q_i} \tag{4}$$

is the apparent acceleration of the substrate due to thermal motion of membrane i, with effective mass m_i.

III. TRAMPOLINE-ON-MEMBRANE (TOM) ACCELEROMETER

To explore the dual-membrane accelerometer concept, we fabricated the device shown in Fig. 1(c), consisting of a 2.5 × 2.5 mm^2, 75-nm-thick Si_3N_4 "trampoline" suspended opposite a square membrane of similar dimensions [16] on a 0.2-mm-thick Si chip (see Methods). Si_3N_4 trampolines have been studied before as *local* force sensors [12]. Here, instead, the trampoline serves as a test mass for acceleration of the chip, to which the relatively stiff square membrane is rigidly attached. The trampoline we study has a 200-μm-wide pad and 4-μm-wide tethers, with fillets tailored to optimize the Q of the fundamental trampoline mode [12,17,18]. For these dimensions, the fundamental resonance frequency of the trampoline is $\omega_1 = 2\pi \times 40$ kHz, the fundamental resonance of the underlying square membrane is $\omega_2 = 2\pi \times 180$ kHz, and the effective mass and Q factor of the trampoline are $m_1 \approx 12$ ng [15] and $Q_1 = 1.1 \times 10^7$, respectively, implying a thermal acceleration noise of $\sqrt{S_a^{\text{th}}} = 0.56\ \mu\text{g}/\sqrt{\text{Hz}}$.

As summarized in Fig. 2, we conducted a series of experiments to characterize the performance of the TOM device as an accelerometer. For these experiments, the device was housed in a high-vacuum ($< 10^{-7}$ mbar) chamber and probed through a viewport with a tunable diode laser (Newport TLB-6716) centered at $\lambda \sim 850$ nm. The laser was intensity stabilized using an electro-optic modulator to −154 dBc, corresponding to a shot-noise-limited power of 1 mW. For readout, the transmitted field was directed to a low-noise photodetector (Thorlabs PDA36A) and the photocurrent was recorded with a 24-bit digitizer (National Instruments PXI-4461).

We first studied the performance of the TOM device as an optical cavity, by recording its transmission $\mathcal{T}$ versus laser wavelength λ as shown in Fig. 2(a). Comparing to the Airy function $\mathcal{T}(\lambda) = (1 + F\sin^2(4\pi d/\lambda))^{-1}$ [19], we infer an effective membrane spacing of $d = 201\ \mu$m and a finesse coefficient of $F = 4R/(1-R)^2 \approx 2$. These values agree well the specified Si-chip thickness and the predicted membrane reflectivity of $R \approx 0.3$ based on a refractive index of $n = 2.0$, implying that the dual-membrane etalon behaves like an impedance-matched Fabry-Perot cavity with a finesse $\mathcal{F} \approx \pi\sqrt{F}/2 \approx 2.2$.

We then attempted to characterize the acceleration susceptibility $\chi(\omega)$ of the TOM device, using driven response measurements. To record displacement x, the laser was

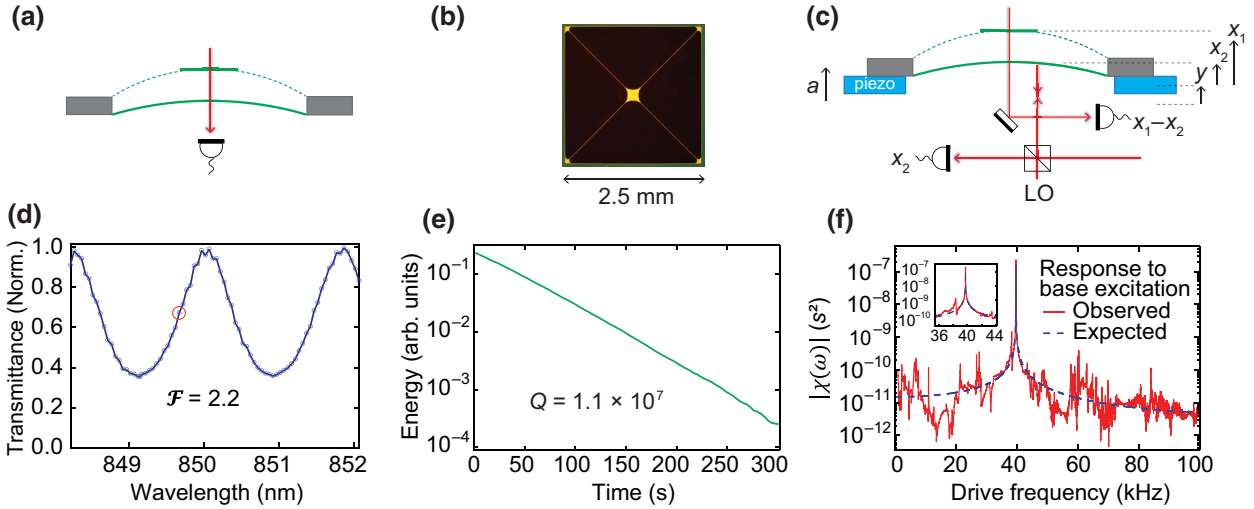

FIG. 2. Characterization of the dual-membrane accelerometer. (a),(d) Optical transmission versus wavelength for a laser scanned near 850 nm. Fitting the interference fringe to an Airy function yields a finesse of 2.2. Readout is performed near the fringe midpoint, highlighted by a red circle. (b) Optical micrograph of the trampoline membrane and (e) energy ringdown of its fundamental flexural mode. Fitting to an exponential yields a Q of 1.1×10^7. (c) Scheme for characterizing the response of the dual-membrane accelerometer (see main text) to a base excitation. (f) Measurement of the response at frequencies below the fundamental resonance of the rigid membrane (180 kHz). Near the 40-kHz trampoline resonance, the response is approximated by the mechanical susceptibility of the trampoline alone.

tuned to the side of the fringe [red circle in Fig. 2(a)] and the transmitted power was monitored in real time. A piezo located beneath the chip was used to apply a sinusoidal test acceleration. To estimate the resonant response, a ringdown measurement was performed by transiently exciting the trampoline, yielding $Q = 1.1 \times 10^7$ as shown in Fig. 1(b). The broadband susceptibility was characterized as shown in Fig. 1(c) by performing a swept-sine measurement. To account for structural resonances of the chip and the piezo, for this measurement, the trampoline-membrane displacement x was normalized to an independent homodyne measurement of the square membrane's displacement x_2. We found that the broadband susceptibility agrees qualitatively well with Eq. (2); however, only over a fractional bandwidth of approximately 20% near the trampoline resonance is it free from spurious features. As the device was designed especially for resonant sensing, we focus on this region for the remainder of this report.

In Fig. 3 we present measurements characterizing the acceleration sensitivity of the TOM device, focusing on a 15-kHz wide frequency window centered on the trampoline resonance. We first note that, while low finesse, the high ideality of the dual-membrane cavity makes it well suited to quantum-limited displacement readout. We confirmed this as shown in Fig. 3(a) by recording the spectral density of the side-of-fringe photocurrent for several different transmitted optical powers P_{out}. To calibrate each spectrum in displacement units, the noise peak at the lowest P_{out} is bootstrapped to the thermal noise model $S_x^{\text{th}}(\omega) = |\chi_1(\omega)|^2 S_a^{\text{th}}(\omega)$ and at higher powers the calibration is scaled by P_{out}^2 [15]. (We estimate a calibration uncertainty of approximately 10% due to uncertainties in m_1 and T, as corroborated by an independent calibration using the fringe slope, presented within the Supplemental Material [15].) In Fig. 3(b), the noise floor is compared to the quantum noise model [15]

$$S_x^{\text{imp}} = \frac{hc\lambda}{6\eta P_{\text{out}}\mathcal{F}^2}. \tag{5}$$

At low powers, $P_{\text{out}} \lesssim 1$ mW, the noise floor agrees well with Eq. (5) with an efficiency of $\eta \approx 33\%$ (accounting for both optical loss and tranduction nonideality). At high powers, $P_{\text{out}} > 1$ mW, the noise floor saturates to an extraneous level of $\sqrt{S_x^{\text{imp}}} \approx 7 \times 10^{-15}/\sqrt{\text{Hz}}$, consistent with the noise floor of our laser intensity servo.

Chip acceleration spectra inferred from the displacement measurements in Fig. 3(a) are shown in Fig. 3(c). Each acceleration spectrum is obtained by dividing the displacement spectrum by the model transfer function $|\chi(\omega)|^2$. The observed inverted lineshape has two components: thermal motion of the trampoline, which masquerades as a frequency independent chip acceleration (solid gray line), and imprecision noise, which has the shape of the inverse susceptibility (dashed gray line). The intersection of these components defines the bandwidth over which the measurement is thermal-noise-limited (gray shaded region), and is approximately the product of the mechanical damping rate $\gamma = \omega_1/Q$ and the peak

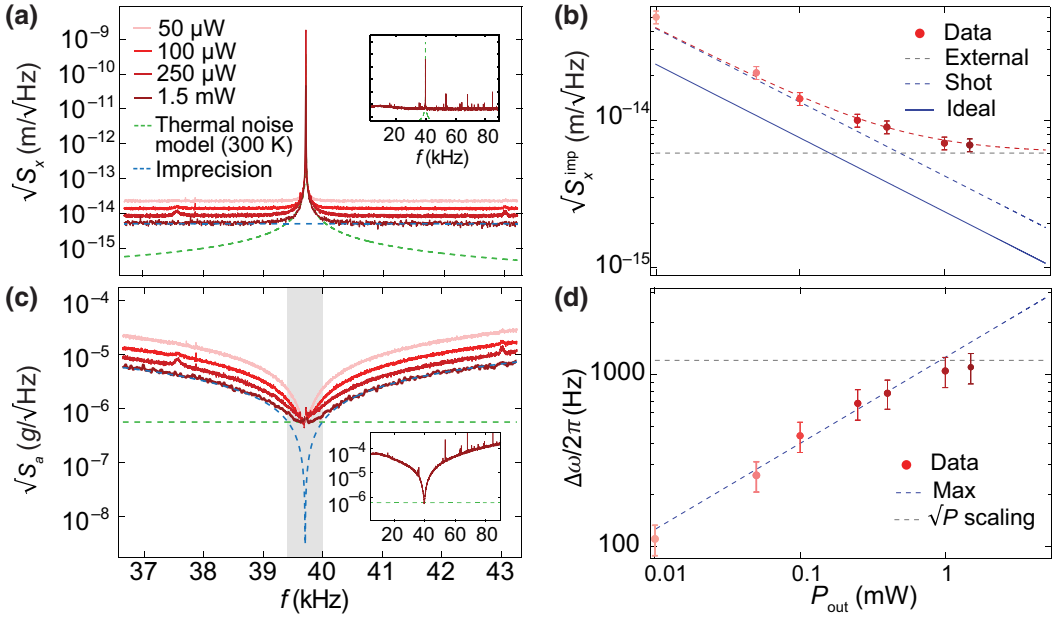

FIG. 3. Displacement and acceleration sensitivity. (a) Apparent trampoline-membrane displacement versus output power, calibrated using the thermal noise peak for the fundamental trampoline mode at 40 kHz. A broadband plot is shown in the inset. (b) Noise floor S_x^{imp} of data in (a) versus optical power, P_{out}. Dashed and solid blue lines are models for shot noise [Eq. (5)] with efficiencies of 33% and 100%, respectively. Dashed red line is a model that includes shot noise and an extraneous imprecision noise of 7.0×10^{-15} m/$\sqrt{\mathrm{Hz}}$ (dashed gray line) (c) Apparent acceleration of the Si chip, inferred by dividing the data in (a) by the acceleration susceptibility [Eqs. (1)–(3)]. The gray shaded region indicates the thermal-noise-limited bandwidth $\delta\omega$ for $P_{\mathrm{out}} = 1.5$ mW. (d) Thermal-noise-limited bandwidth versus optical power. Dashed blue and gray lines correspond to models for shot noise [Eq. (6)] and a constant extraneous noise [dashed gray line in (b)].

thermal-to-imprecision-noise ratio [15]

$$\Delta\omega \approx \gamma \sqrt{\frac{S_x^{\mathrm{th}}(\omega_1)}{S_x^{\mathrm{imp}}}}. \tag{6}$$

As shown in Fig. 3(e), $\Delta\omega$ increases with power as long as the readout is shot-noise-limited, ultimately saturating at $\Delta\omega \approx 2\pi \times 1$ kHz due to extraneous noise. Over this range, we infer a thermal-noise-limited acceleration sensitivity of $S_a^{\mathrm{th}} = 0.6\ \mu\mathrm{g}/\sqrt{\mathrm{Hz}}$ based on the trampoline $Q \times m$ product. A moderate increase in the finesse, to $\mathcal{F} = 100$ (e.g., using a PtC membrane [9]), could in principle extend this sensitivity to baseband ($\Delta\omega \approx \omega_1$). On the other hand, notably, the large resonant thermal motion of the trampoline $S_x^{\mathrm{th}}(\omega_1) = 4k_BTQ/m\omega_1^3 = (1.0\ \mathrm{nm}/\sqrt{\mathrm{Hz}})^2$ implies that thermal-noise-limited measurements $\Delta\omega > \gamma$ are possible with as little as femtowatts of optical power in the current Fresnel reflection ($\mathcal{F} \sim 1$) arrangement.

IV. RADIATION-PRESSURE-ENHANCED ACCELEROMETRY

The preceding results show that a pair of high-Q Si_3N_4 membranes can be used realize an optomechanical accelerometer with sub-μg sensitivity over a bandwidth of kilohertz, using milliwatts of optical power. We now turn our attention to a unique opportunity afforded by the simultaneous high force sensitivity of the membranes, which enables their intrinsic mechanical susceptibility to be overwhelmed by radiation pressure back-action, leading to optical stiffening and damping [6]. Previous work on COM accelerometers cited radiation pressure as a future tool for enhanced sensing [1,4]. For example, optical damping (either passive [5] or active [21]) might be used to rectify instabilities and nonlinearities [22–24], yielding improved dynamic range; while optical stiffening [23,25] might be used to increase bandwidth or (via dissipation dilution [26,27]) sensitivity. However, the use of relatively large, low-Q test masses, and a focus on baseband sensing, has limited the implementation of these approaches in optomechanical accelerometers to date.

The TOM device was designed with radiation pressure in mind as a tool for incoherent acceleration sensing, inspired by recent proposals to search for a weak inertial force produced by ultralight dark matter [13,14]. Towards this end, we follow the approach of Gavartin *et al.* [28] to show that radiation-pressure cold damping (feedback cooling) can be used to reduce the resolving time for an incoherent acceleration measurement. The strategy of Ref. [28] involves using Bartlett's method to estimate the area $\langle x^2 \rangle$ of the thermal noise peak, which is proportional to S_a^{th}. The standard deviation of the estimate $\Delta\langle x^2 \rangle$

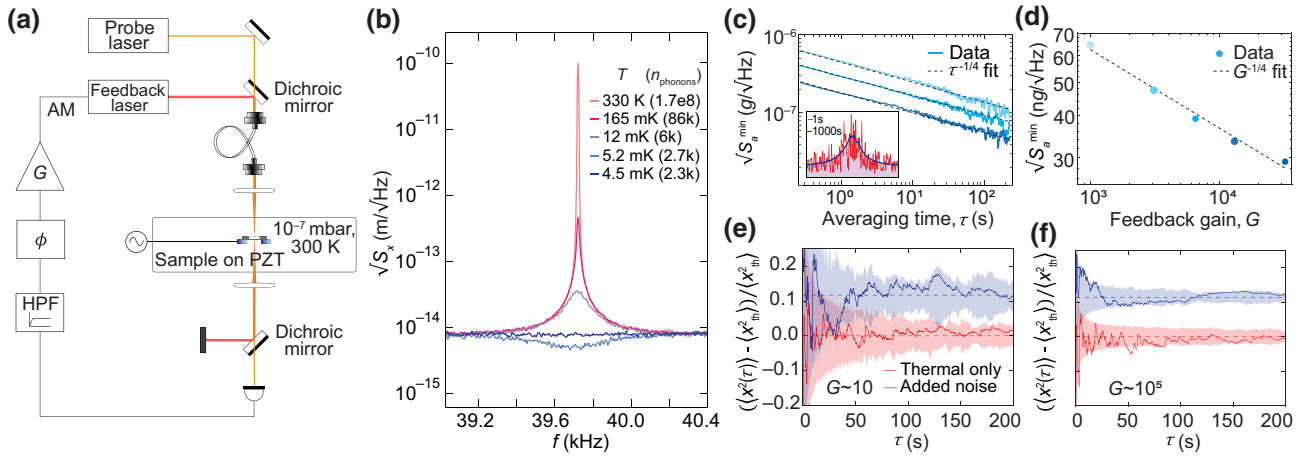

FIG. 4. Radiation-pressure-enhanced optomechanical accelerometry. (a) Experimental setup: an 850-nm laser is used to probe the TOM device in transmission using the side-of-the-fringe technique. The processed photosignal—high pass filtered (HPF), phase shifted (ϕ), and amplified (G)—is used to modulate the intensity of an auxiliary 650-nm laser for radiation-pressure feedback. (b) Feedback cooling of the fundamental trampoline mode from room temperature to an effective temperature of 4 mK. (Squashing below the noise floor corresponds to an increase in the effective temperature [20].) (c) Thermal acceleration resolution at 40 kHz as a function of averaging time τ for several feedback gains. Inset: displacement spectrum for different τ. The thermal acceleration resolution is proportional to the variance in the spectrum magnitude. (d) Acceleration resolution at $\tau = 1000$ s for different feedback gains. (e),(f) Acceleration resolution versus time with (blue) and without (red) external white noise applied with a piezo, for both low (e) and high (f) feedback cooling gain. Solid lines represent the long time average and shaded region indicates the confidence bounds. These plots show that an incoherent acceleration signal can be distinguished from thermal acceleration at much shorter averaging times when the feedback damping (gain) is higher.

determines the smallest incoherent acceleration that can be resolved atop thermal noise, *viz.*

$$S_a^{\min}(\tau, \gamma_{\rm eff}) = \frac{\Delta\langle x^2\rangle}{\int_{-\infty}^{\infty}|\chi_{\rm eff}(\omega)|^2 d\omega/2\pi} \simeq \frac{S_a^{\rm th}}{(\gamma_{\rm eff}\tau)^{1/2}}, \quad (7)$$

where τ is the total measurement (averaging) time, $\chi_{\rm eff}(\omega) \approx \beta_1/(\omega_1^2 - \omega^2 - i\omega\gamma_{\rm eff})$ is the effective (closed-loop) acceleration susceptibility, and $\gamma_{\rm eff}$ and $T_{\rm eff}$ are the effective damping rate and temperature of the mechanical mode, respectively, satisfying $\gamma_{\rm eff}T_{\rm eff} = \gamma T$ for cold damping [21]. Equations (6) and (7) imply that τ can be reduced by as much as the initial signal-to-noise ratio $\sqrt{S_x^{\rm th}(\omega_1)/S_x^{\rm imp}}$ by cold damping to the noise floor, $\gamma_{\rm eff} = \Delta\omega$. While this result has been shown to only recover the performance of an optimal Wiener filter estimation strategy [29], it holds a practical advantage in that the Wiener filter must approximate the intrinsic mechanical susceptibility [30,31], a task which is difficult to accomplish electronically [32] for a high-Q resonator.

In Fig. 4, we present an experiment demonstrating incoherent acceleration sensing at the level of 50 ng/$\sqrt{\rm Hz}$ by cold damping the fundamental trampoline mode of the TOM device. The probe laser is fixed at $P_{\rm out} = 650\ \mu$W (yielding approximately equal to 30 K of photothermal heating [15]) and a radiation-pressure damping force, $F_{\rm RP} = -G\gamma\dot{x}$, is supplied by a weak secondary laser ($\lambda \approx 650$ nm, $P_{\rm out} = 50\ \mu$W) whose amplitude is modulated with a phase-shifted copy of the photosignal using a preamplifier (Stanford Research Systems SR560) and a delay line. The increased net damping, $\gamma_{\rm eff} = (1+G)\gamma$, reduces the effective temperature of the flexural mode from $T_0 \approx 330$ K (i.e., $\langle n\rangle = k_B T_0/\hbar\omega_1 \approx 1.7\times10^8$ thermal phonons) to an effective temperature of [17,20]

$$T = \frac{1}{1+G}T_0 + \frac{G^2}{(1+G)}T_{\rm imp} \geq 2\sqrt{T_0 T_{\rm imp}}, \quad (8)$$

where $T_{\rm imp} = T_0 S_x^{\rm imp}/S_x^{\rm th}(\omega_1)$ is the effective measurement temperature [20,21]. As shown in Fig. 4(b), $\sqrt{S_x^{\rm imp}} = 7$ fm/$\sqrt{\rm Hz}$ allows us to cool the mode to $T \approx 4$ mK ($\langle n\rangle \approx 2\times10^3$) using an optimal gain of $G = 1.5\times10^5$. Applying the area estimation method for a variety of intermediate gains, we confirm that $\sqrt{S_a^{\rm min}} \propto (G\tau)^{-1/4}$ as shown in Figs. 4(c) and 4(d). At the optimal gain setting, an apparent acceleration resolution of $\sqrt{S_a^{\rm min}} \approx 50$ ng/$\sqrt{\rm Hz}$ is achieved with a measurement time of 200 s, limited by the onset of drift in experimental controls [15].

Finally, as a demonstration (following Refs. [28,30]), we used a piezo to apply an approximately 180 ng/$\sqrt{\rm Hz}$ incoherent acceleration to the chip, smaller than the thermal acceleration by a factor of approximately 3. As shown in Figs. 4(e) and 4(f), the area averaging technique was used to estimate the total noise with feedback gains of $G \sim 10$

and $G \sim 10^5$, respectively. Shaded regions highlight the uncertainty of the estimate. For lower gain [Fig. 4(e)], it takes visibly longer (approximately 100 s) to resolve the external acceleration noise from thermal noise. For higher gain [Fig. 4(f)], the resolving time is significantly smaller (approximately 1 s); however, the signal-to-noise ratio (the vertical distance between the red and blue data) remains unchanged since the feedback is linear.

V. SUMMARY AND OUTLOOK

We have presented a platform for optomechanical accelerometry based on a pair of vertically integrated Si_3N_4 membranes with different stiffnesses, forming an optical cavity. Devices based on this platform are simple to fabricate, can achieve sub-μg sensitivity over a bandwidth of kilohertz, and can be actively controlled using radiation-pressure feedback. As a proof of principle, we studied a "trampoline-on-membrane" device in which a 40-kHz nanotrampoline with a Q-m product of 100 mg is integrated opposite a 180-kHz square membrane on a common 200 μm Si chip, forming a finesse $\mathcal{F} \approx 2$ cavity. Despite its low finesse, the high ideality of the cavity enabled shot-noise-limited readout of the membrane separation at the level of fm/$\sqrt{\text{Hz}}$, yielding sensitivity to sub-μg/$\sqrt{\text{Hz}}$ chip accelerations over a bandwidth of 1 kHz centered at the trampoline resonance, limited by thermal noise. Radiation-pressure feedback was then used to cool the trampoline's fundamental vibration to an effective temperature of 4 mK. While not affecting the acceleration sensitivity, we confirm that cold damping enables emulation of an optimal filter, allowing us to resolve externally applied chip accelerations at the level of 50 ng/$\sqrt{\text{Hz}}$ in an integration time of 200 s. In the future, we envision integrating PtC mirrors into both membranes [33] to achieve $\mathcal{F} \sim 100$; in principle, this will enable a 100-fold reduction in displacement noise, extending thermal-noise-limited acceleration sensitivity to baseband. Operating the device in a dilution refrigerator could enable quantum back-action-limited acceleration measurements [13,34] and give access to sensitivities relevant to the search for fundamental weak forces. For example, fixing the device to a germanium or beryllium base would give access to equivalence principle violating (material-dependent) accelerations hypothetically produced by dark photon dark matter [13].

VI. METHODS

Fabrication of the TOM device is simple and scalable [35]: starting with a double-side-polished Si wafer, Si_3N_4 is deposited on both sides using low-pressure chemical vapor deposition. The trampoline is patterned on one side using photolithography, and the double-membrane structure is released with a single KOH wet-etch step. The square membrane serves as both an etch stop and a turbulence shield. Finally, the released structure is dried using a gradual dilution process [12] followed by critical point drying. Similar structures have been fabricated with embedded PtC mirrors [33] and a straightforward extension to PnC membranes [10,11] is conceivable, including arrays of such structures distributed over a wafer.

ACKNOWLEDGMENTS

This work is supported by NSF Grant No. ECCS-1945832. D.J.W. acknowledges additional support from the NSF Convergence Accelerator Program under Grant No. 2134830 and from the Northwestern University Center for Fundamental Physics and the John Templeton Foundation through a Fundamental Physics Grant. The authors thank Christian Pluchar for help designing the optical readout system and Utkal Pandurangi and Felipe Guzmán for useful conversations about the development of the device. A.R.A. acknowledges support from a CNRS-UArizona iGlobes fellowship. Finally, the reactive ion etcher used for this study was funded by an NSF MRI Grant, No. ECCS-1725571.

CONTRIBUTIONS

A.R.A. conceived of, simulated, fabricated, and initially characterized the device. M.D.C. designed and conducted all experiments, and performed all data analysis. M.D.C. and D.J.W. co-wrote the paper and Supplemental Material, with assistance from A.R.A. D.J.W. oversaw the project.

[1] A. G. Krause, M. Winger, T. D. Blasius, Q. Lin, and O. Painter, A high-resolution microchip optomechanical accelerometer, Nat. Photon. **6**, 768 (2012).
[2] F. Guzmán Cervantes, L. Kumanchik, J. Pratt, and J. M. Taylor, High sensitivity optomechanical reference accelerometer over 10 khz, Appl. Phys. Lett. **104**, 221111 (2014).
[3] B. J. Reschovsky, D. A. Long, F. Zhou, Y. Bao, R. A. Allen, T. W. LeBrun, and J. J. Gorman, Intrinsically accurate sensing with an optomechanical accelerometer, Opt. Exp. **30**, 19510 (2022).
[4] Y. L. Li and P. Barker, Characterization and testing of a micro-g whispering gallery mode optomechanical accelerometer, J. Lightwave Technol. **36**, 3919 (2018).
[5] T. J. Kippenberg and K. J. Vahala, Cavity optomechanics: back-action at the mesoscale, Science **321**, 1172 (2008).
[6] M. Aspelmeyer, T. J. Kippenberg, and F. Marquardt, Cavity optomechanics, Rev. Mod. Phys. **86**, 1391 (2014).
[7] F. Zhou, Y. Bao, R. Madugani, D. A. Long, J. J. Gorman, and T. W. LeBrun, Broadband thermomechanically limited sensing with an optomechanical accelerometer, Optica **8**, 350 (2021).

[8] R. St-Gelais, S. Bernard, C. Reinhardt, and J. C. Sankey, Swept-frequency drumhead optomechanical resonators, ACS Photon. **6**, 525 (2019).
[9] R. A. Norte, J. P. Moura, and S. Gröblacher, Mechanical resonators for quantum optomechanics experiments at room temperature, Phys. Rev. Lett. **116**, 147202 (2016).
[10] Y. Bao, J. Gorman, and J. Lawall, in *Frontiers in Optics* (Optical Society of America, 2020), p. FW7D–2.
[11] Y. Tsaturyan, A. Barg, E. S. Polzik, and A. Schliesser, Ultracoherent nanomechanical resonators via soft clamping and dissipation dilution, Nat. Nanotechnol. **12**, 776 (2017).
[12] C. Reinhardt, T. Müller, A. Bourassa, and J. C. Sankey, Ultralow-Noise SiN Trampoline Resonators for Sensing and Optomechanics, Phys. Rev. X **6**, 021001 (2016).
[13] J. Manley, M. D. Chowdhury, D. Grin, S. Singh, and D. J. Wilson, Searching for Vector Dark Matter with an Optomechanical Accelerometer, Phys. Rev. Lett. **126**, 061301 (2021).
[14] D. Carney, G. Krnjaic, D. C. Moore, C.A. Regal, G. Afek, S. Bhave, B. Brubaker, T. Corbitt, J. Cripe, N. Crisosto, and A. Geraci, Mechanical quantum sensing in the search for dark matter, Quantum Sci. Technol. **6**, 024002 (2021).
[15] See Supplemental Material at http://link.aps.org/supplemental/10.1103/PhysRevApplied.19.024011 for theoretical and experimental details.
[16] The underlying square membrane is slightly smaller, 2.2×2.2 mm^2, due to the 54.7° angle at which the Si(100) substrate is etched by KOH (see Sec. VI).
[17] C. M. Pluchar, A. R. Agrawal, E. Schenk, and D. J. Wilson, Towards cavity-free ground-state cooling of an acoustic-frequency silicon nitride membrane, Appl. Opt. **59**, G107 (2020).
[18] P. Sadeghi, M. Tanzer, S. L. Christensen, and S. Schmid, Influence of clamp-widening on the quality factor of nanomechanical silicon nitride resonators, J. Appl. Phys. **126**, 165108 (2019).
[19] L. L. Sánchez-Soto, J. J. Monzón, and G. Leuchs, The many facets of the Fabry–Perot, Eur. J. Phys. **37**, 064001 (2016).
[20] M. Poggio, C. Degen, H. Mamin, and D. Rugar, Feedback Cooling of a Cantilever's Fundamental Mode Below 5 mK, Phys. Rev. Lett. **99**, 017201 (2007).
[21] D. Kleckner and D. Bouwmeester, Sub-kelvin optical cooling of a micromechanical resonator, Nature **444**, 75 (2006).
[22] G. I. Harris, U. L. Andersen, J. Knittel, and W. P. Bowen, Feedback-enhanced sensitivity in optomechanics: Surpassing the parametric instability barrier, Phys. Rev. A **85**, 061802 (2012).
[23] T. Corbitt, Y. Chen, E. Innerhofer, H. Müller-Ebhardt, D. Ottaway, H. Rehbein, D. Sigg, S. Whitcomb, C. Wipf, and N. Mavalvala, An All-Optical Trap for a Gram-Scale Mirror, Phys. Rev. Lett. **98**, 150802 (2007).
[24] J. Mertz, O. Marti, and J. Mlynek, Regulation of a microcantilever response by force feedback, App. Phys. Lett. **62**, 2344 (1993).
[25] M. Hossein-Zadeh and K. J. Vahala, Observation of optical spring effect in a microtoroidal optomechanical resonator, Opt. Lett. **32**, 1611 (2007).
[26] T. Corbitt, C. Wipf, T. Bodiya, D. Ottaway, D. Sigg, N. Smith, S. Whitcomb, and N. Mavalvala, Optical Dilution and Feedback Cooling of a Gram-Scale Oscillator to 6.9 mK, Phys. Rev. Lett. **99**, 160801 (2007).
[27] K.-K. Ni, R. Norte, D. Wilson, J. Hood, D. Chang, O. Painter, and H. Kimble, Enhancement of Mechanical Q Factors by Optical Trapping, Phys. Rev. Lett. **108**, 214302 (2012).
[28] E. Gavartin, P. Verlot, and T. J. Kippenberg, A hybrid on-chip optomechanical transducer for ultrasensitive force measurements, Nat. Nanotechnol. **7**, 509 (2012).
[29] A. Vinante, M. Bonaldi, F. Marin, and J. Zendri, Dissipative feedback does not improve the optimal resolution of incoherent force detection, Nat. Nanotechnol. **8**, 470 (2013).
[30] G. I. Harris, D. L. McAuslan, T. M. Stace, A. C. Doherty, and W. P. Bowen, Minimum Requirements for Feedback Enhanced Force Sensing, Phys. Rev. Lett. **111**, 103603 (2013).
[31] A. Pontin, M. Bonaldi, A. Borrielli, F. Cataliotti, F. Marino, G. Prodi, E. Serra, and F. Marin, Detection of weak stochastic forces in a parametrically stabilized micro-optomechanical system, Phys. Rev. A **89**, 023848 (2014).
[32] E. Gavartin, P. Verlot, and T. Kippenberg, Reply to "Dissipative feedback does not improve the optimal resolution of incoherent force detection", Nat. Nanotechnol. **8**, 692 (2013).
[33] C. Gärtner, J. P. Moura, W. Haaxman, R. A. Norte, and S. Gröblacher, Integrated optomechanical arrays of two high reflectivity SiN membranes, Nano Lett. **18**, 7171 (2018).
[34] N. Kampel, R. Peterson, R. Fischer, P.-L. Yu, K. Cicak, R. Simmonds, K. Lehnert, and C. Regal, Improving Broadband Displacement Detection with Quantum Correlations, Phys. Rev. X **7**, 021008 (2017).
[35] A. R. Agrawal and D. J. Wilson, Membrane-based optomechanical accelerometer, methods of making the same and systems using the same, (W.O. Patent No. WO/2022/174112A1, 2022), https://patentscope.wipo.int/search/en/detail.jsf?docId=WO2022174112.